



# 4D Flow MR: Insights into Aortic Blood Flow Characteristics

# 28

Florian von Knobelsdorff-Brenkenhoff  
and Alex J. Barker

## 28.1 What Is 4D Flow MR?

4D flow MRI is an extension of the well-established 2D phase contrast sequence commonly used to measure blood flow velocities in the vasculature. In its simplest form, the 2D flow approach is used clinically to measure unidirectional blood flow through imaging planes placed perpendicular to the long axis of a vessel. 4D flow MRI is a further extension of the technique that does not only collect velocity data though, or in the imaging plane, but rather in all three principal directions ( $x$ ,  $y$ ,  $z$ ) over a volumetric field of view. The volumetric acquisition, which includes a spatially and temporally resolved three-directional velocity field, is commonly referred to in the literature as 4D flow MRI [1]. Regardless of the implementation (4D or 2D flow), phase-contrast MRI is rooted in the use of a bipolar magnetic gradient to cause proton spin phase shifts proportional to their displacement over time (in the case of blood, the phase shifts are caused by water protons). Given that these phase

shifts are acquired during a specific time window, knowledge of the bulk proton displacement within a voxel can be used to obtain a spatially resolved velocity field of the corresponding fluid. When combined with ECG gating, time-resolved velocities can be derived on a voxel-by-voxel basis, and their temporal evolution can be represented over one (virtual) heart cycle. Integration of the temporal and spatial velocity field over the cross section of the target vessel allows for the calculation of blood flow rate and volume. This approach is commonly used in clinical routine, for example, with 2D flow, to quantify aortic regurgitation volumes or the ratio of pulmonary to systemic stroke volume to diagnose a shunt [2].

The same approach as that used with 2D flow can be used with a 4D flow acquisition, but with additional coverage of the adjacent vasculature. Similar results have been found at both 1.5 and 3 T [3], although the signal-to-noise ratio is higher at 3 T with visibly better image contrast. As a general rule of thumb, contrast agents are not required but are known to enhance the intraluminal signal and improve image quality and velocity to noise ratio [4]. For planning, a 3D field of view is typically prescribed to cover the targeted area, such as one covering the thoracic aorta. During acquisition, data are collected with ECG gating to correct for cardiac movement and to order the  $k$ -space lines with respect to the cardiac cycle. Respiratory motion is commonly compensated using a navigator technique. One approach is to continuously

---

F. von Knobelsdorff-Brenkenhoff (✉)  
Department of Cardiology,  
Clinic Agatharied, Academic Teaching Hospital,  
Ludwig-Maximilians-University Munich,  
Norbert-Kerkel-Platz, Munich, Germany  
e-mail: [Florian.vonKnobelsdorff@khagatharied.de](mailto:Florian.vonKnobelsdorff@khagatharied.de)

A. J. Barker  
Department of Radiology, Feinberg School of  
Medicine, Northwestern University, Chicago, IL, USA  
e-mail: [alex.barker@northwestern.edu](mailto:alex.barker@northwestern.edu)

monitor the movement of the diaphragm at end diastole and acquire image data at a predefined acceptance window for the diaphragm location. As a result, respiratory motion is minimized by limiting the acquisition to a small range of acceptable positions, which will be used to reconstruct the final images, while the remainder of the data is rejected. Depending on the size of the field of view, efficiency of the navigator, heart rate, and acceleration mode of the sequence, image acquisition generally takes 8–20 min. The resulting image dataset typically contains magnitude images depicting the anatomy, and three phase-contrast datasets that represent the principal velocity directions, which when combined, represents the 3D flow field (Fig. 28.1). Typical imaging parameters for the thoracic aorta include a spatial resolution of 2–2.5 mm<sup>3</sup> and a temporal resolution of 35–50 ms [5]. To visualize and extract quantitative flow information, the dataset requires further post-processing, which is accomplished with a diverse set of software solutions, and is dependent on user requirements. For exam-

ple, most post-processing solutions allow for flow visualization of both the blood flow velocity and direction using color-coded pathlines or streamlines (Fig. 28.2). Qualitatively, streamline and pathline visualization aids in the ability to localize complex flow phenomena, such as identifying the presence of helices and vortices caused by abnormalities in vascular structure (Fig. 28.3) [6]. Furthermore, the quantification of flow velocity as well as a variety of derived parameters like flow volumes, wall shear stress, pulse wave velocity, and energy loss is possible; however some of these parameters may require specialized software or programming expertise. Nonetheless, most analysis software will allow for the user to take advantage of the main benefit of 4D flow MRI, that is, the ability to retrospectively prescribe imaging measurement planes in the 3D dataset. In contrast, the traditional approach of 2D flow is limited to the original predefined imaging planes (Fig. 28.2). While image acquisition and data post-processing of 4D flow data could be time-consuming in the past, recent software and

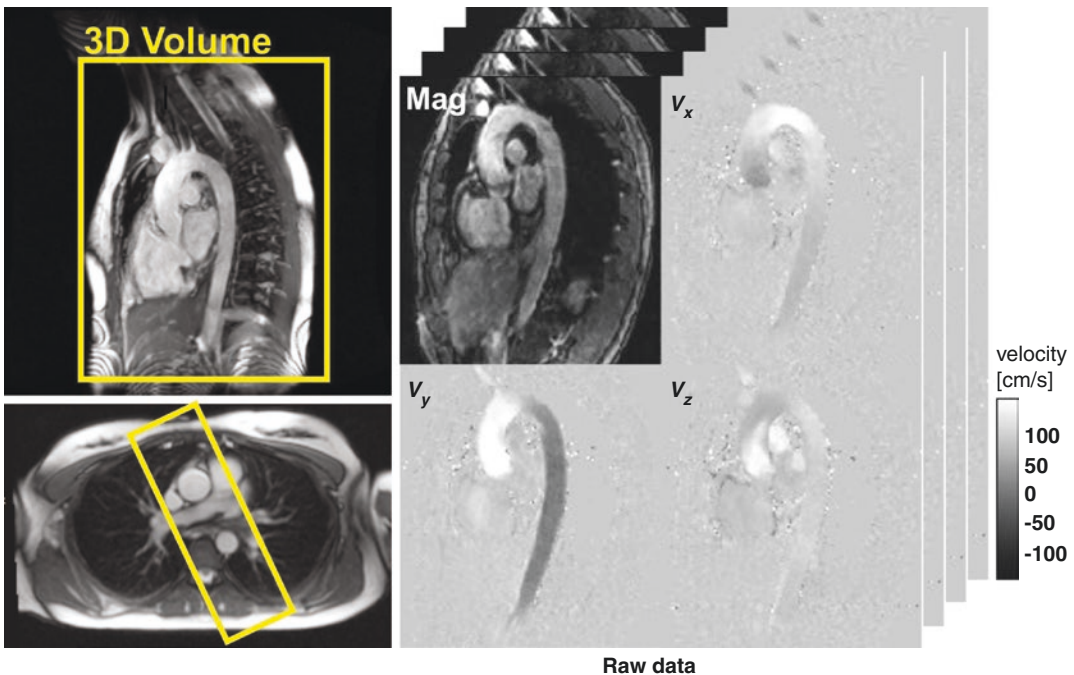


**Fig. 28.1** Acquisition planning. A 3D volume (field of view) is selected to cover the target vessel. The 4D flow raw data comprises of magnitude images reflecting the

anatomy and phase images reflecting flow velocities along all three spatial dimensions, three velocity directions, and time in the cardiac cycle (adapted from Markl et al. [5])

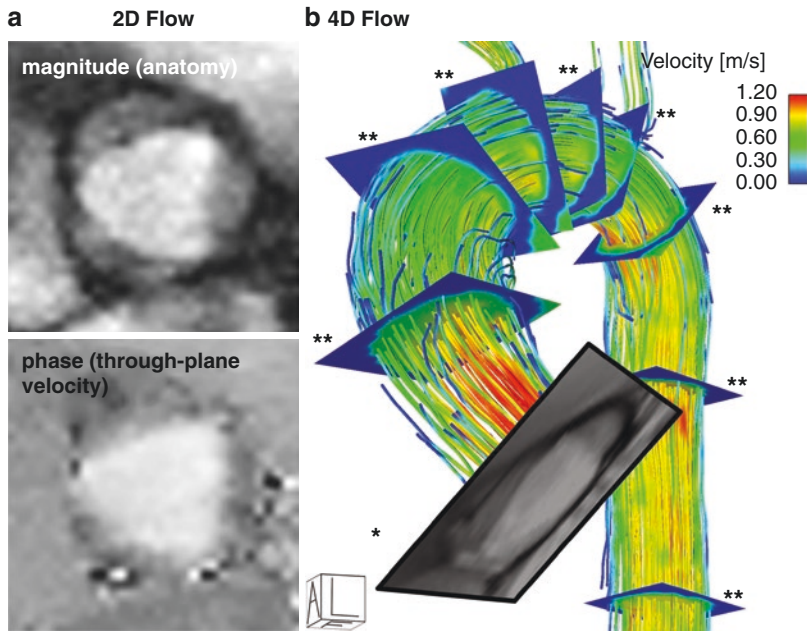


**Fig. 28.2** (a) Visualization of the output from a standard 2D flow acquisition in comparison to (b) a 4D flow acquisition in a normal healthy volunteer (the 2D flow acquisition plane is illustrated on the 4D flow volume with the “\*” label). The additional cross-sectional planes (labeled “\*\*”) illustrate the ability to retrospectively interrogate the velocity field anywhere in the imaging field of view.

The color-coded velocity streamlines represent the velocity magnitude of the characteristic systolic flow pattern in the thoracic aorta. For the healthy aorta and aortic valve, the streamlines are cohesive and oriented in the longitudinal direction of the vessel during systole. Little evidence of vortical or helical flow is visible at this time point (adapted from Barker et al. [12])

hardware developments are quickly enabling the workup of 4D flow data in a time window appropriate for the clinical setting. In this context, the 2014 European Society for Cardiology guidelines for aortic diseases comment that 4D flow provides the unique opportunity to visualize and measure blood flow patterns and highlights that quantitative parameters such as pulse wave velocity and wall shear stress can be determined [7].

## 28.2 4D Flow in the Normal Aorta

During systole, the high-velocity ejection jet tends to migrate to the outer curvature, as visualized by peak velocity streamlines. Later in systole, the streamlines curve posterolaterally, back toward the inner curvature in a right-handed helix in the ascending aorta and arch [8]. In the proximal descending aorta, velocities increase where streamlines tend to separate from the inner curva-

ture, converging slightly toward the outer wall. During early diastole, retrograde flow occurs along the inner curvatures of both the ascending and proximal descending arch, which may contribute to diastolic filling of the coronary arteries [9].

In preliminary examinations of flow in the normal aorta, estimates of wall shear stress (the tangential frictional force at the vessel wall) have been reported. This force, which is computed using the blood velocity gradient at the wall as obtained from 4D flow MRI and an assumption of constant blood viscosity, is a known mechano-transduction factor affecting atherosclerosis, cellular signaling, and vascular remodeling [10]. Of particular interest is the range of normal wall shear stress expressed in the healthy individual as a function of vascular region. For example, in one such study, the mean absolute time-averaged wall shear stress ranged between  $0.25 \pm 0.04$  N/m<sup>2</sup> and  $0.33 \pm 0.07$  N/m<sup>2</sup> and incorporated a substantial circumferential component ( $-0.05 \pm 0.04$  to

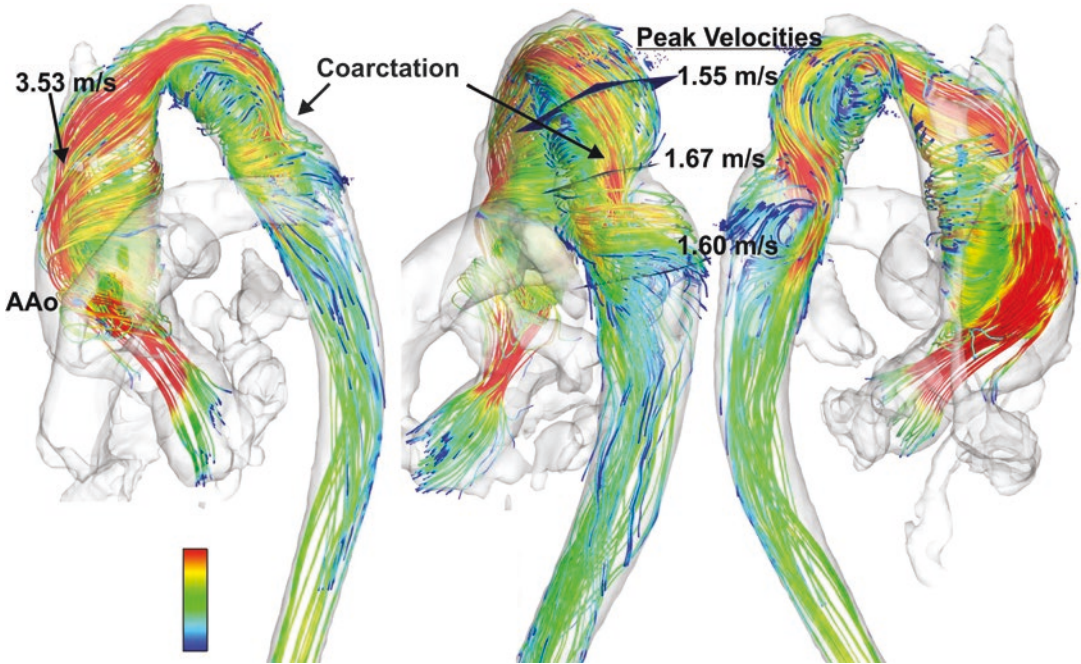


**Fig. 28.3** 3D streamline visualization of thoracic aortic systolic blood flow as assessed by 4D flow in a patient with a bicuspid aortic valve with fusion of the right- and left-coronary leaflets and aortic coarctation at the proximal descending aorta. There is a posteriorly directed, high-velocity flow jet in the ascending aorta (AAo) with

associated right-handed helix formation. Complex aortic geometry near the coarctation results in vortex formation proximal to the coarctation, a right-handed helix distal to the coarctation, and flow acceleration through the aortic narrowing (adapted from Markl et al. [5])

$0.07 \pm 0.02 \text{ N/m}^2$ ) [11]. At each level of the thoracic aorta, a regional location was identified with the lowest absolute wall shear stress and highest oscillatory shear index, which differed significantly from the mean values within the plane. Interestingly, the observed distribution of atherogenic low wall shear stress and high oscillatory shear index closely resembled typical locations of atherosclerotic lesions at the inner aortic curvature and supraaortic branches. Additional independent 4D flow studies involving healthy individuals have corroborated these insightful wall shear stress findings [12–15]. As a result, data collected with the 4D flow technique have provided compelling evidence to corroborate the hemodynamic hypothesis that low and oscillating wall shear stress promotes the development and progression of regional atherosclerotic lesions in the aorta.

Additional 4D flow post-processing techniques have demonstrated the ability to measure the propagation of the systolic flow wavefront along the length of the aorta. The velocity of the flow wavefront,

known as pulse wave velocity, is a known marker for global vascular compliance and has shown to be feasibly estimated using 4D flow data [16, 17]. The 4D flow approach to estimate pulse wave velocity is a promising method to investigate the change of vascular compliance in the presence of aging, atherosclerosis, and cardiovascular disease.

### 28.3 4D Flow in the Dilated Aorta

The guidelines for aortic disease and valvular disease cite aortic dilation as a risk factor for aortic dissection [18, 19]. The concept of aorta size as a risk factor for dissection is somewhat controversial since, on an individual basis, aortic dissection occurs in subjects with normal aorta sizes, and the majority of patients with aortic dilatation will never suffer from aortic dissection. Therefore, personalized measures to improve the understanding of aortic remodeling and to risk-stratify beyond diameter thresholds are desired to improve



patient care. With this in mind, 4D flow has been explored in patients with aortic dilatation to identify abnormal flow patterns and wall shear stress distribution. For example, Biegling et al. compared patients with aortic dilatation to healthy controls and found that ascending aortic dilatation was associated with increased diastolic wall shear stress, decreased systolic to diastolic wall shear stress ratio, and delayed onset of peak wall shear stress. In addition, temporally averaged wall shear stress was increased, and peak systolic wall shear stress was decreased. The maximum wall shear stress in patients with aortic dilatation was on the anterior wall of the ascending aorta. Vortical flow with highest velocities along the anterior wall and

increased helical flow during diastole were observed in patients [13]. Bürk et al. also studied patients with dilated ascending aorta and compared them to age-matched subjects. Thereby, the incidence and strength of supraphysiologic-helix and vortex flow in the ascending aorta were significantly higher in patients with dilated ascending aorta than in controls. Interestingly, the extent and incidence of ascending aortic helix and vortex flow were associated with significant differences in ascending aortic diameters. Peak systolic wall shear stress in the ascending aorta and aortic arch was significantly lower in patients with dilated ascending aorta (Fig. 28.4). The ascending aortic diameter positively correlated to time to peak sys-

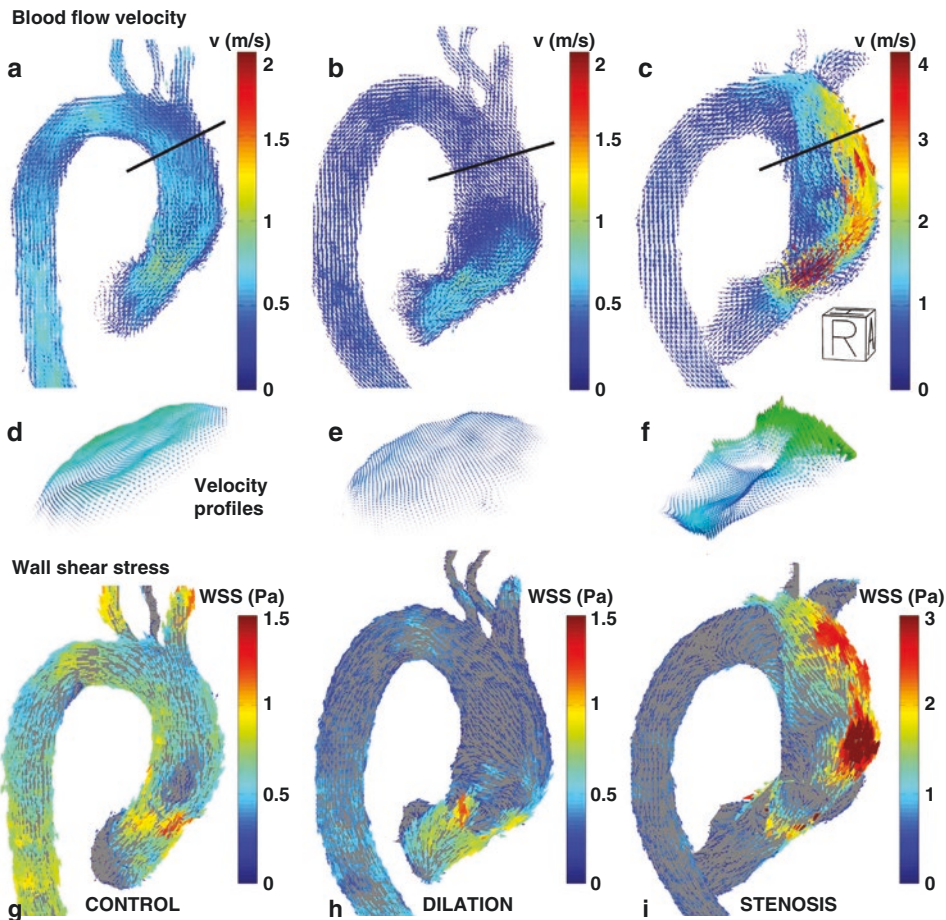


**Fig. 28.4** Visualization of blood flow velocity vectors in a typical control aorta (a), dilated aorta (b), and aorta with severe valve stenosis (c). Cross-sectional velocity profiles are shown at the level of the black lines in (d), (e), and (f). The

corresponding 3D WSS pattern is shown below these subjects (g), (h), and (i). Note that the velocity and WSS color bar for the stenosis subject are two times higher than for the other two examples (adapted from van Ooij et al. [22])

tolic velocities and oscillatory shear index and inversely correlated to peak systolic wall shear stress. Peak systolic wall shear stress was significantly lower in ascending aortic aneurysms at the right and outer curvature within the ascending aorta and proximal arch [15]. These findings indicate that specific hemodynamic alterations exist in the dilated aorta compared to the normal aorta. In the future, these insights may help elucidate specific flow patterns that increase risk for adverse cardiovascular events, such as dissection.

---

## 28.4 4D Flow in Aortic Stenosis

Post-stenotic aortic dilation has been linked to altered mechanical stress on the wall of the ascending aorta caused by flow disturbance downstream of a stenotic lesion [20]. Normal systolic flow in the ascending aorta is cohesive, with fastest flow in the vessel center, and shear stress evenly distributed around the aortic circumference. In patients with post-stenotic dilation, however, systolic flow is often eccentric and displaced from the centerline toward the vessel wall and follows a helical path through the ascending aorta. Consequently, wall shear stress is asymmetrically elevated. This pattern was observed in subjects with aortic stenosis both with normal and with dilated ascending aorta, which supports the argument that the abnormal flow is caused by the valve itself and not by the dilated aorta (Fig. 28.4) [21, 22].

The preceding descriptions focus on blood flow downstream from the aortic valve and provide general information regarding the impact of aortic stenosis on flow pattern abnormalities and flow environment near the ascending aorta wall. On the ventricle side of the valve, blood flow caused by aortic stenosis will have an upstream impact on function and cardiac burden. One parameter that may gain importance in this regard is the measurement of irreversible energy losses caused by frictional effects across a valvular obstruction and altered downstream flow. These losses exist in both laminar and turbulent flow regimes, with the turbulent regime typically being an order of magnitude greater compared to

the laminar regime. As a result, recent efforts have attempted to estimate turbulent kinetic energy from 4D flow datasets noninvasively to detect regions of elevated flow turbulence and thus irreversible energy loss. This is important as irreversible energy loss (manifested as pressure loss) in post-stenotic flow is an important determinant of the hemodynamic significance of aortic stenosis and cardiac afterload. Post-stenotic energy loss is largely caused by dissipation of turbulent kinetic energy into heat and manifests in the clinic as a measurable pressure loss during invasive catheterization. In a recent study, Dyverfeldt et al. measured the turbulent kinetic energy in patients with aortic stenosis. It was significantly higher in stenosis patients than in normal volunteers, and the peak total turbulent kinetic energy in the ascending aorta was strongly correlated to indexed pressure loss as obtained by echocardiography [23]. Similarly, using 4D flow datasets, Barker et al. quantified the laminar component of viscous energy loss in the ascending aorta and found elevated losses in patients with aortic stenosis compared with healthy volunteers. In addition, those patients with dilated aortas and no valve disease displayed significantly higher viscous losses than healthy individuals, although lower than aortic stenosis patients. These data reinforce the concept that cardiac afterload is increased due to abnormal flow, aortic size, and valve morphology in these subjects [24].

---

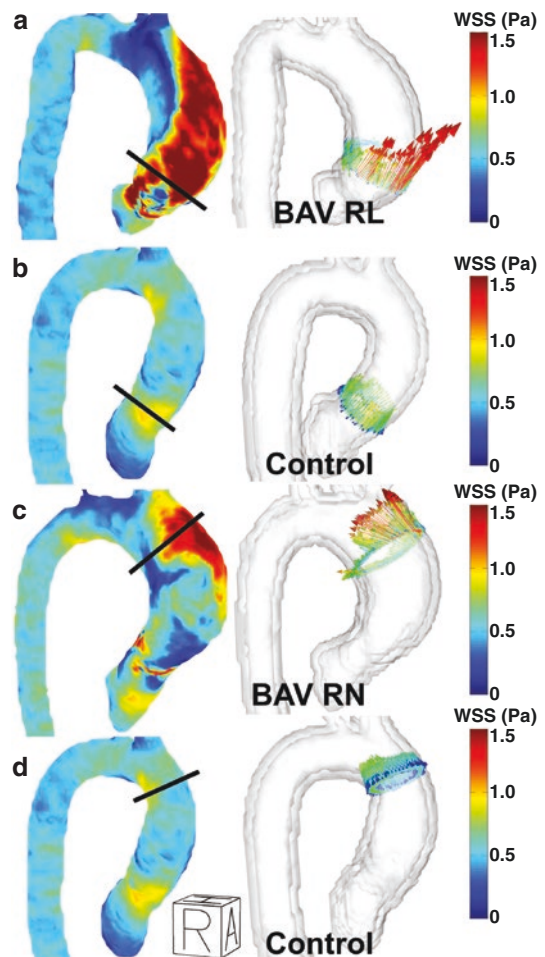
## 28.5 4D Flow in Bicuspid Aortic Valve

Bicuspid aortic valve disease is associated with ascending aortic dilatation and increased risk of aortic dissection [7]. This association is attributed to a genetic predisposition leading to malformation of the valve and the aortic wall. Furthermore, unfavorable shear forces near the vessel wall can change endothelial function and possibly create areas at risk for vascular remodeling. The permanent hemodynamic burden due to the abnormal valve geometry is thought to be a contributor to aortic abnormalities in patients with bicuspid aortic valve [25]. The latter argument has recently

been supported by studies using 4D flow to visualize and analyze the blood flow in the ascending aorta. Barker et al. measured the impact of bicuspid aortic valve disease on the distribution of regional aortic wall shear stress compared with age-/aorta size-controlled cohorts with tricuspid valves. Wall shear stress patterns in the ascending aorta of bicuspid aortic valve patients were significantly elevated, independent of stenosis severity (Fig. 28.5). The observation of right-anterior ascending aorta wall/jet impingement in patients corresponded to regions with elevated wall shear stress. Alternative jetting patterns were observed depending on the fusion type of the bicuspid aortic valve [12]. Meierhofer et al. confirmed these results in another series [14]. In a study with almost a hundred of patients with bicuspid aortic

valve disease by Bissell et al., patients with bicuspid aortic valve had predominantly abnormal right-handed helical flow in the ascending aorta, larger ascending aortas, and higher rotational (helical) flow, systolic flow angle, and systolic wall shear stress compared with healthy volunteers. Bicuspid aortic valve with right-handed flow and right-noncoronary cusp fusion showed more severe flow abnormalities and larger aortas than right-left cusp fusion. Patients with bicuspid aortic valve with normal flow patterns had similar aortic dimensions and wall shear stress when compared to healthy volunteers. Younger patients with bicuspid aortic valve showed abnormal flow patterns, but no aortic dilation. Both of these observations support the potential importance of flow pattern in the pathogenesis of aortic dilation [26].

**Fig. 28.5** Distribution of peak wall shear stress projected on a 3D segmentation of the aorta (left column) and wall shear stress vectors (right column) in planes placed at the regions of maximum wall shear stress for (a) bicuspid aortic valve (BAV) as compared to the same location in a healthy control (b) (adopted from [22]). Eccentric WSS at the sinus and proximal arch is illustrated for two phenotypes of BAV patients (a, c) as compared to healthy controls (b, d). One example is a BAV patient with a fusion of the right-left (BAV RL) coronary leaflets, and the other is a BAV patient with a fusion of the right and noncoronary (BAV RN) leaflets



Hope et al. addressed the effect of abnormal blood flow in the ascending aorta on the aortic growth rate in patients with bicuspid aortic valve. They analyzed serial MR or CT studies. The growth rates of patients with bicuspid aortic valve were significantly higher than those of controls. Those patients with abnormal flow patterns demonstrated significantly higher growth rates than those with normal flow. The authors state that imaging biomarkers such as these could be used to identify and risk-stratify patients in whom clinically significant aortic disease is likely to develop [27].

Figure 28.3 shows a 4D flow case of bicuspid aortic valve disease that illustrates the potential of 4D flow to capture the impact of localized pathologies (bicuspid aortic valve disease, here in association with coarctation) on complex changes in aortic hemodynamics affecting the entire thoracic aorta. In addition, the complete volumetric coverage provides the user with the ability to identify the optimal location for retrospective quantification of clinically relevant parameters such as peak jet flow velocities distal to the bicuspid aortic valve and within the coarctation [5].

---

## 28.6 4D Flow in Aortic Coarctation

4D flow can help evaluate collateral blood flow as a potential measure of hemodynamic significance in patients with aortic coarctation. Additionally, distorted flow patterns in the descending aorta after coarctation repair such as marked helical and vortical flow in regions of post-stenotic dilation were reported [28, 29]. This distorted pattern becomes even more marked in the presence of BAV. In a recent study, 4D flow data were used to calculate pressure fields in patients with aortic coarctation, which showed a close agreement to catheterization as the clinical gold standard, and may eventually replace this invasive procedure in the future [30].

---

## 28.7 4D Flow After Aortic Surgery

Postoperative 4D flow MRI can provide information regarding the ability of the surgeon to restore blood flow in the aorta to that representing a

healthy physiologic flow pattern. Along these lines, 4D flow has been performed to analyze blood flow in the thoracic aorta of patients after valve-sparing aortic root replacement. In a study by Markl et al., 12 patients after David reimplantation using a cylindrical tube graft (T. David-I) and two versions of neosinus recreation (T. David-V and T. David-V-Smod) were included. Systolic vortices were seen in both coronary sinuses of all volunteers. Comparable coronary vortices were detected in all operated patients. Vorticity was minimal in the noncoronary cusp in T. David-I repairs but was prominent in T. David-V noncoronary graft pseudosinuses. Retrograde flow and helicity were found in all patients but were not distinguishable from normal values in the T. David-V-Smod patients [31]. Another study applied 4D flow to characterize the aortic blood flow in patients following valve-sparing aortic root replacement compared with presurgical cohorts matched by tricuspid and bicuspid valve morphology, age, and presurgical aorta size. They found that after valve-sparing aortic root replacement, the helical flow was reduced and less eccentric compared to presurgical control subjects, but there was a trend toward higher systolic flow acceleration as a surrogate measure of reduced aortic compliance [32].

---

## 28.8 4D Flow After Aortic Valve Surgery

Aortic remodeling after aortic valve replacement (AVR) may be influenced by postoperative blood flow patterns in the ascending aorta. The feasibility of 4D flow in the proximity of heart valve prosthesis has been demonstrated to perform reliably in *in vitro* flow phantoms [33]. In an *in vivo* pilot study, 4D flow was applied to describe ascending aortic flow characteristics after various types of AVR: mechanical prostheses, stented bioprostheses, stentless bioprostheses, and autografts. The study demonstrated that the flow characteristics in the ascending aorta after each type of AVR were different from native aortic valves and moreover differed between the various types of AVR. Additionally, mechanical prostheses showed the most distinct vorticity compared to



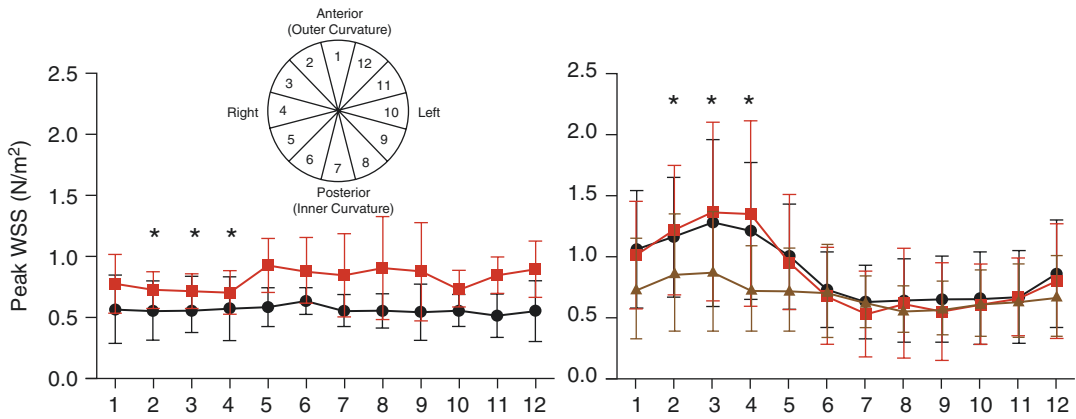


**Fig. 28.6** Distribution of peak wall shear stress in the mid-ascending aorta after various types of aortic valve surgery (adapted from [34])

controls, while stented bioprostheses exhibited the most distinct helicity. Instead of physiologic central flow, all stented, stentless, and mechanical prostheses showed eccentric flow jets mainly directed toward the right-anterior aortic wall. Stented and stentless prostheses showed an asymmetric distribution of peak wall shear stress along the aortic circumference, with significantly increased local wall shear stress where the flow jet impinged on the aortic wall (Fig. 28.6). Local wall shear stress was higher in stented and stentless compared to autografts and controls. Autografts exhibited lower wall shear stress than controls [34].

A similar approach has been used in recipients of a transcatheter aortic valve implantation (TAVI). Thereby, TAVI and stented bioprostheses exhibited a similar pattern of asymmetric wall shear stress distribution in the ascending aorta, while the appearance of vortices and helices was stronger in those with stented bioprosthesis compared to TAVI [35].

ECG trigger time will cause signal loss or artifact in the corresponding regions. The presence of signal loss or artifacts is especially relevant for regions with high degrees of turbulence and strong intravoxel velocity variations (which can manifest as intravoxel dephasing). Besides turbulent flow, the typical temporal resolution of a 4D flow sequence is on the order of 40 ms, which can miss local peaks or fluctuations of wall shear stress. However, this disadvantage (compared to echocardiography) is balanced with the added ability to visualize the full magnitude of eccentric velocity jets, contrary to echocardiography, which is limited to resolving velocities collinear with the beamline. Finally, one must consider that the resolution of the acquisition is finite. Thus, the spatial resolution of 4D flow data is insufficient to resolve small-scale boundary layers or arterial velocity profiles in small vessels (<6–8 mm). Wall shear stress values should therefore be considered estimates of the shear rate of the blood near the vessel wall [9].

## 28.9 Limitations of 4D Flow

4D flow MRI requires the collection of k-space lines over a number of ECG-gated heartbeats. Thus, care must be taken to note that the observed flow features have been measured over a number of cardiac cycles. Additionally, beat to beat variations in the velocity field that occur at the same

## 28.10 Conclusion

4D flow MR is a promising technique for detailed qualitative and quantitative assessment of cardiovascular hemodynamics. The method allows for the evaluation of a large body of hemodynamic parameters that can be derived from the 4D flow data. Initial reports on the clinical application of

these parameters are promising, e.g., in aortic or aortic valve disease and after intervention at the aorta or aortic valve. It is still unclear, however, which parameters are most suitable for the evaluation of different types of cardiovascular pathologies. Longitudinal studies are thus warranted to investigate the predictive value of novel 4D flow hemodynamic parameters and their utility to complement existing clinical risk stratification and therapy management strategies [5].

## References

1. Markl M, Kilner PJ, Ebbers T. Comprehensive 4D velocity mapping of the heart and great vessels by cardiovascular magnetic resonance. *J Cardiovasc Magn Reson*. 2011;13:7.
2. Myerson SG. Heart valve disease: investigation by cardiovascular magnetic resonance. *J Cardiovasc Magn Reson*. 2012;14:7.
3. Strecker C, Harloff A, Wallis W, Markl M. Flow-sensitive 4D MRI of the thoracic aorta: comparison of image quality, quantitative flow, and wall parameters at 1.5 T and 3 T. *J Magn Reson Imaging*. 2012;36:1097–103.
4. Bock J, Frydrychowicz A, Stalder AF, et al. 4D phase contrast MRI at 3 T: effect of standard and blood-pool contrast agents on SNR, PC-MRA, and blood flow visualization. *Magn Reson Med*. 2010;63:330–8.
5. Markl M, Schnell S, Barker AJ. 4D flow imaging: current status to future clinical applications. *Curr Cardiol Rep*. 2014;16:481.
6. Lorenz R, Bock J, Barker AJ, et al. 4D flow magnetic resonance imaging in bicuspid aortic valve disease demonstrates altered distribution of aortic blood flow helicity. *Magn Reson Med*. 2014;71:1542–53.
7. Erbel R, Aboyans V, Boileau C, et al. 2014 ESC Guidelines on the diagnosis and treatment of aortic diseases: document covering acute and chronic aortic diseases of the thoracic and abdominal aorta of the adult. The Task Force for the Diagnosis and Treatment of Aortic Diseases of the European Society of Cardiology (ESC). *Eur Heart J*. 2014;35:2873–926.
8. Kilner PJ, Yang GZ, Wilkes AJ, Mohiaddin RH, Firmin DN, Yacoub MH. Asymmetric redirection of flow through the heart. *Nature*. 2000;404:759–61.
9. Markl M, Geiger J, Kilner PJ, et al. Time-resolved three-dimensional magnetic resonance velocity mapping of cardiovascular flow paths in volunteers and patients with Fontan circulation. *Eur J Cardiothorac Surg*. 2011;39:206–12.
10. Malek AM, Alper SL, Izumo S. Hemodynamic shear stress and its role in atherosclerosis. *JAMA*. 1999;282:2035–42.
11. Frydrychowicz A, Stalder AF, Russe MF, et al. Three-dimensional analysis of segmental wall shear stress in the aorta by flow-sensitive four-dimensional-MRI. *J Magn Reson Imaging*. 2009;30:77–84.
12. Barker AJ, Markl M, Burk J, et al. Bicuspid aortic valve is associated with altered wall shear stress in the ascending aorta. *Circ Cardiovasc Imaging*. 2012;5:457–66.
13. Bieging ET, Frydrychowicz A, Wentland A, et al. In vivo three-dimensional MR wall shear stress estimation in ascending aortic dilatation. *J Magn Reson Imaging*. 2011;33:589–97.
14. Meierhofer C, Schneider EP, Lyko C, et al. Wall shear stress and flow patterns in the ascending aorta in patients with bicuspid aortic valves differ significantly from tricuspid aortic valves: a prospective study. *Eur Heart J Cardiovasc Imaging*. 2013;14:797–804.
15. Burk J, Blanke P, Stankovic Z, et al. Evaluation of 3D blood flow patterns and wall shear stress in the normal and dilated thoracic aorta using flow-sensitive 4D CMR. *J Cardiovasc Magn Reson*. 2012;14:84.
16. Markl M, Wallis W, Brendecke S, Simon J, Frydrychowicz A, Harloff A. Estimation of global aortic pulse wave velocity by flow-sensitive 4D MRI. *Magn Reson Med*. 2010;63:1575–82.
17. Dyverfeldt P, Ebbers T, Lanne T. Pulse wave velocity with 4D flow MRI: systematic differences and age-related regional vascular stiffness. *Magn Reson Imaging*. 2014;32:1266–71.
18. Nishimura RA, Otto C. 2014 ACC/AHA valve guidelines: earlier intervention for chronic mitral regurgitation. *Heart*. 2014;100:905–7.
19. Hiratzka LF, Bakris GL, Beckman JA, et al. 2010 ACCF/AHA/AATS/ACR/ASA/SCA/SCAI/SIR/STS/SVM guidelines for the diagnosis and management of patients with thoracic aortic disease: executive summary. A report of the American College of Cardiology Foundation/American Heart Association Task Force on Practice Guidelines, American Association for Thoracic Surgery, American College of Radiology, American Stroke Association, Society of Cardiovascular Anesthesiologists, Society for Cardiovascular Angiography and Interventions, Society of Interventional Radiology, Society of Thoracic Surgeons, and Society for Vascular Medicine. *Catheter Cardiovasc Interv*. 2010;76:E43–86.
20. Wilton E, Jahangiri M. Post-stenotic aortic dilatation. *J Cardiothorac Surg*. 2006;1:7.
21. Hope MD, Dyverfeldt P, Acevedo-Bolton G, et al. Post-stenotic dilation: evaluation of ascending aortic dilation with 4D flow MR imaging. *Int J Cardiol*. 2012;156:e40–2.
22. van Ooij P, Potters WV, Nederveen AJ, et al. A methodology to detect abnormal relative wall shear stress on the full surface of the thoracic aorta using four-dimensional flow MRI. *Magn Reson Med*. 2015;73:1216–27.
23. Dyverfeldt P, Hope MD, Tseng EE, Saloner D. Magnetic resonance measurement of turbulent kinetic energy for the estimation of irreversible pres-

- sure loss in aortic stenosis. *JACC Cardiovasc Imaging*. 2013;6:64–71.
24. Barker AJ, van Ooij P, Bandi K, et al. Viscous energy loss in the presence of abnormal aortic flow. *Magn Reson Med*. 2014;72:620–8.
  25. Barker AJ, Markl M. The role of hemodynamics in bicuspid aortic valve disease. *Eur J Cardiothorac Surg*. 2011;39:805–6.
  26. Bissell MM, Hess AT, Biasioli L, et al. Aortic dilation in bicuspid aortic valve disease: flow pattern is a major contributor and differs with valve fusion type. *Circ Cardiovasc Imaging*. 2013;6:499–507.
  27. Hope MD, Wrenn J, Sigovan M, Foster E, Tseng EE, Saloner D. Imaging biomarkers of aortic disease: increased growth rates with eccentric systolic flow. *J Am Coll Cardiol*. 2012;60:356–7.
  28. Hope MD, Meadows AK, Hope TA, et al. Clinical evaluation of aortic coarctation with 4D flow MR imaging. *J Magn Reson Imaging*. 2010;31:711–8.
  29. Frydrychowicz A, Markl M, Hirtler D, et al. Aortic hemodynamics in patients with and without repair of aortic coarctation: in vivo analysis by 4D flow-sensitive magnetic resonance imaging. *Investig Radiol*. 2011;46:317–25.
  30. Riesenkampff E, Fernandes JF, Meier S, et al. Pressure fields by flow-sensitive, 4D, velocity-encoded CMR in patients with aortic coarctation. *JACC Cardiovasc Imaging*. 2014;7:920–6.
  31. Markl M, Draney MT, Miller DC, et al. Time-resolved three-dimensional magnetic resonance velocity mapping of aortic flow in healthy volunteers and patients after valve-sparing aortic root replacement. *J Thorac Cardiovasc Surg*. 2005;130:456–63.
  32. Semaan E, Markl M, Malaisrie SC, et al. Haemodynamic outcome at four-dimensional flow magnetic resonance imaging following valve-sparing aortic root replacement with tricuspid and bicuspid valve morphology. *Eur J Cardiothorac Surg*. 2014;45:818–25.
  33. von Knobelsdorff-Brenkenhoff F, Dieringer MA, Greiser A, Schulz-Menger J. In vitro assessment of heart valve bioprostheses by cardiovascular magnetic resonance: four-dimensional mapping of flow patterns and orifice area planimetry. *Eur J Cardiothorac Surg*. 2011;40:736–42.
  34. von Knobelsdorff-Brenkenhoff F, Trauzeddel RF, Barker AJ, Gruettner H, Markl M, Schulz-Menger J. Blood flow characteristics in the ascending aorta after aortic valve replacement—a pilot study using 4D-flow MRI. *Int J Cardiol*. 2014;170:426–33.
  35. Trauzeddel F, Loebe U, Barker A, et al. Blood flow pattern in the ascending aorta after TAVI and conventional aortic valve replacement: analysis using 4D-flow MRI. *Int J Cardiovasc Imaging*. 2016;32:461–7.